Some lava flows may not have been as thick as they appear

Jonas Katona[1,2], Xiaojing Fu[1,3], Tushar Mittal[1,4], Michael Manga[1], and Stephen Self[1].

[1]University of California Berkeley, Berkeley, CA, United States
[2]Yale University, New Haven, CT, United States
[3]California Institute of Technology, Pasadena, CA, United States
[4]Massachusetts Institute of Technology, Cambridge, MA, United States

Key Points:

- Lava flows can heat and melt underlying flows if the flows are hot enough;
- Superimposed lava flows can merge if erupted in close enough succession;
- Macroscopic structures may not reflect the original flow thicknesses.

Corresponding author: Jonas Katona, `jonas.katona@yale.edu`

Corresponding author: Xiaojing Fu, `rubyfu@caltech.edu`

Abstract

Individual lava flows in flood basalt provinces are composed of sheet pāhoehoe lobes and the 10-100 m thick lobes are thought to form by inflation. Quantifying the emplacement history of these lobes can help infer the magnitude and temporal dynamics of these prehistoric eruptions. Here we use a phase-field model to describe solidification and re-melting of sequentially-emplaced lava flows to explore additional processes that may lead to thick flows. We calibrate model parameters using field measurements at Makaopuhi lava lake. We vary the thickness of individual flows and the time interval between eruptions to study the interplay between thermal evolution, flow thickness and emplacement frequency. Our theoretical analysis shows that, if the time between emplacement is sufficiently short, reheating and re-melting may merge sequentially emplaced flows — making flows appear thicker than they actually were. Our results suggest that fused flows could be another mechanism that creates apparently thick lava flows.

Plain Language Summary

The observation of thick basaltic lava flows has long been explained by inflation. Here we explore an additional mechanism that could explain the formation of thick lava flows, where a sequence of thinner lobes that are emplaced on top of each other could fuse into one large flow. Our theoretical analysis suggests the formation of a thick flow by merging can occur if the flows are emplaced relatively close to each other in time.

1 Introduction

Continental flood basalt (CFB) province eruptions contain the largest ($> 1{,}000$ km^3, Bryan and Ernst (2008); Self et al. (2014)) and longest (~ 1000 km; Self et al. (2008)) lava flows. Since CFBs are frequently coeval with severe environmental perturbations including mass extinctions, ocean anoxic events and hyperthermal events (Clapham & Renne, 2019), understanding the physical process and time-scale of flow field emplacement would help quantify the release of volcanic gases that have environmental impacts (e.g., CO_2, SO_2). Despite decades of work, however, the tempo of CFB eruptions remains poorly quantified.

CFB lava flow fields are composed of 5 - 100 m thick dominantly pāhoehoe lobes (Self et al., 1998). Given the general lack of large lava tubes in CFBs (Kale et al., 2020; Self et al., 1998), the primary process hypothesized for creating thick flows is the formation of pāhoehoe lobes by inflation. If the quasi-continuous magma flux into individual lava lobes is sufficient, the solidifying surface crust can continuously rise due to increasing pressure (Hon et al., 1994a; Hoblitt et al., 2012). If the lateral magma pressure is large enough, the flow can propagate laterally by sporadic breakouts (Hon et al., 1994a; Kauahikaua et al., 1998). This process has been observed in modern meter-scale Icelandic and Hawaiian lobes (Self et al., 1998). In addition, the lobe structures in CFB flows have similar internal characteristics as Hawaiian inflated lobes (Vye-Brown et al., 2013). The maximal final inflated lobe thickness in Hawaiian flows, however, is only 10 - 15 m (Kauahikaua et al., 1998), which is smaller than many CFB flows (up to 80-100 m, Puffer et al. (2018); Self et al. (2021)). Furthermore, lava flow inflation has been shown to require pulsating eruptive conditions that may not always be possible (Rader et al., 2017). Thus, a fundamental question remains: how do CFB flows become so thick?

In this study, we explore an additional process that can lead to apparently thick flows, in which the final flow is an amalgamation of numerous smaller lobes, piled on top of each other quickly enough to remelt the intervening solidified crust (Basu et al., 2012, 2013). In Section 2, we describe a phase-field model for lava flow cooling. We then simulate solidification of a single flow and two sequentially emplaced flows using the model in one dimension. In Section 3, we outline three distinct regimes characterized by inter-lobe cooling. We finally compare our results with observations to assess whether remelting can help explain the thick CFB flows. Our results are used to put lower bounds on how quickly CFB flow fields were emplaced in order to preserve multiple lobes within a single flow field.

2 A phase-field model of lava solidification

The phase-field framework is a mathematical approach to describe systems out of thermodynamic equilibrium (Anderson et al., 1998). It was first introduced in the context of solidification processes and phase transitions of pure or multi-component materials (Cahn & Hilliard, 1958; Boettinger et al., 2002). The framework allows us to evolve the solidification front as part of the solution to the system of partial differential equations, avoiding the need for explicit treatment and tracking of the moving interface as is traditional done in the Stefan problem (Anderson et al., 1998). Here, we consider a simplified model of lava solidification where we track the binary solidification of lava through a phase variable, denoted ϕ ($\phi = 1$ for melt and $\phi = 0$ for solid phase), and the corresponding temperature, denoted T. In a phase-field framework, the evolution of ϕ and T can be described with the following system of coupled, nonlinear partial differential equations:

$$\tau \partial_t \phi + \nabla \cdot \left(-\omega_\phi^2 \nabla \phi\right) = -g'(\phi) - \frac{L}{H}\frac{(T - T_m)}{T_m} P'(\phi), \tag{1}$$

$$\partial_t T + \nabla \cdot (-\alpha \nabla T) = \frac{L}{c_p} h'(\phi)\, \partial_t \phi, \tag{2}$$

where T_m is the melting temperature of the lava, $\alpha = k\rho^{-1}c_p^{-1}$ is the thermal diffusion coefficient (k thermal conductivity, ρ density, c_p specific heat), ω_ϕ characterizes the length of the interfacial transition zone, τ characterizes the time scale of solidification across the interface, and H is the energy barrier. The above equations are completed with the following auxiliary functions: $g(\phi) = \phi^2(1-\phi)^2$; $P(\phi) = (3 - 2\phi)\phi^2$; $h(\phi) = P(\phi)$ (Provatas & Elder, 2010). To obtain parameter values of the model that accurately characterize solidification dynamics of basaltic lava, we adopt typical values of thermal properties of basaltic melt (Patrick et al., 2004). The phase-field modeling parameters τ and w_ϕ^2 are derived in Text S1 (in the supporting information) using the approach adopted from Kim and Kim (2005) and then calibrated based on field data collected from Makaopuhi lava Lake (Wright & Okamura, 1977; Wright et al., 1972; Wright & Marsh, 2016), as shown in Figure S1. Table 1 summarizes the parameter values used in our study.

We use the phase-field model and parameters to perform two types of simulations of basaltic lava solidification. We first simulate solidification of a single lava lobe of thickness h to obtain the total time t_h it takes to reach complete solidification ($\phi = 0$ everywhere). The results are used to design the second set of simulations, where we simulate sequential emplacement of two lava lobes of equal thickness h, separated by a time period of t_{emp}. We consider h from 0.1m to 20m to explore the behaviors of both thin pāhoehoe lobes (< 1m), as seen in recent Kīlauea eruptions, and thick lobes ($\gg$ 1m), as seen in Columbia River Basalt Group (CRBG) and other Continental Flood Basalts (Self et al., 2021). For the sequential emplacement simulations, we explore nine different emplacement intervals for each thickness. All the simulations are performed in one dimension. The domain initially consists of a substrate that is $4 \times h$ thick with a uniform ground temperature of $T_g = 20°C$. The total domain grows dynamically as lava lobes are emplaced at temperature $T_0 = 1200°C$:

$$\phi(t=0) = \begin{cases} 1 & z \in [0, 4h) \\ 0 & z \in [4h, 5h] \end{cases}, \qquad T(t=0) = \begin{cases} T_g & z \in [0, 4h) \\ T_0 & z \in [4h, 5h] \end{cases}$$

The bottom boundary condition is set to a constant temperature of T_g and always solid, assuming that the deep ground maintains a fixed temperature. The top boundary con-

Table 1. Parameters used for the model.

	Definition	Unit	Values used
L	latent heat of fusion	$\mathrm{J/m^3}$	4×10^5
c_p	specific heat at constant pressure	$\mathrm{J/(m^3 \cdot K)}$	2.57×10^6
k	thermal conductivity	$\mathrm{J/(m} \cdot s \cdot \mathrm{K)}$	9.64×10^{-1}
T_m	melting temperature	$^o\mathrm{C}$	1070
τ	characteristic time of solidification	s	2.90×10^6
α	thermal diffusivity	$\mathrm{m^2/s}$	3.75×10^{-7}
w_ϕ^2	interfacial coefficient	m	1.04×10^{-1}
σ	interfacial energy	$\mathrm{J/m^2}$	5×10^{-1}
β	kinetic coefficient	$\mathrm{m\ Pa/K^2}$	5.6×10^{-8}
H	energy barrier	$\mathrm{J/m^3}$	6.59
h_c	convective heat transfer coefficient of air	$\mathrm{W/(m^2 \cdot K)}$	2.62×10^1
σ_s	Stefan-Boltzmann constant	$\mathrm{W/(m^2 \cdot K^4)}$	5.67×10^{-8}
ε	emissivity of the lava surface		0.6

dition is set to lose heat due to black-body radiation, convection by a fixed wind speed and conduction. We also assume that a crust readily forms at the top of lava surface:

$$\text{Bottom boundary} \quad : \quad \phi = 1; \quad T = T_g; \tag{3}$$

$$\text{Top boundary} \quad : \quad \phi = 1; \quad k\frac{\partial T}{\partial z} = -h_c\left(T - T_s\right) - \sigma_s \varepsilon \left(T^4 - T_s^4\right). \tag{4}$$

Here, $T_s = 30°\mathrm{C}$ is the surface air temperature, h_c, σ_s, and ε are the convective heat transfer coefficient for air flow, Stefan-Boltzmann constant, and the emissivity of the lava surface, respectively. In practice, h_c depends on the wind speed and angle at which it travels with respect to the lava. However, considering that fluctuations in the external environment are on a much smaller timescale compared to the solidification timescale, we assume a constant h_c as shown in Table 1, which corresponds to a wind speed of roughly 2 m/s (Patrick et al., 2004).

We perform the numerical simulations with a 4th-order centered difference discretization in space to properly resolve the phase boundary. We use the AB4-AM4 predictor–corrector method (Atkinson, 1988; Zlatev, 1985) to integrate in time, which allows us to increase time step size while ensuring accuracy for the highly-resolved grid. Because our simulations need to capture temporal dynamics that span from the order of seconds (initial cooling) to years, we also implement adaptive time-stepping as monitored with Milne's device (Atkinson, 1988; Zlatev, 1985; Fujii, 1991) (see also Text S2). We use Ralston's 4th-order Runge-Kutta method (Ralston, 1962) to predict the first four time steps after each change in time step size. The spatial grid size we use Δx roughly scales with h, which balances computational efficiency with numerical precision (see Text S3). In the following section, we describe the results from these numerical studies and discuss their implications for understanding emplacement dynamics of thin and thick lava flows.

3 Results

We perform a total of 153 simulations that explore 17 different lobe thickness ($0.1\mathrm{m} \leq h \leq 20\mathrm{m}$) and nine different emplacement intervals (in months, unless noted otherwise) for each h. Based on these simulations, we have identified three distinct regimes of inter-lobe solidification. These regimes can be delineated based on the ratio between t_{emp} and the conductive time scale (approximated by h^2/α). Below, we describe each regime in detail with examples for the case of $h = 10\mathrm{m}$ lava flows in Figure 1.

In sequence ($t_{\mathbf{emp}} > 0.06h^2/\alpha$): The first lava lobe completely solidifies before the second lobe is emplaced (Figure 1, right). The temporal cooling dynamics of both flows are similar and the bottom flow does not remelt.

In parallel ($0.01h^2/\alpha < t_{\mathbf{emp}} < 0.06h^2/\alpha$): As indicated by the narrowing of both black contours in the top plot and the decreasing melt thickness in the lower plot with time, both lava lobes solidify for overlapping time, but the interface between them does not remelt (Figure 1, middle). Because the bottom flow is hot, the collective cooling of both flows is slower than *in sequence* flows, as indicated by the decrease in slope in Figure 1 (bottom middle).

Fused flow ($0 < t_{\mathbf{emp}} < 0.01h^2/\alpha$): After emplacement, the solidified portion of the lower lava lobe eventually remelts completely, and then both lobes combine to form one large lobe which solidifies as one. For early times, there are four solid-melt interfaces that correspond to the simultaneous solidification of two independent lobes. However, the two interior interfaces disappear at some point, marking the melting and merging of the two lobes. The remelting event is also clear when we track the total melt thickness over time (Figure 1 bottom). After the arrival of the second lobe (indicated by red dot), the total melt thickness increases slightly at some point, corresponding to the remelting that caused a reduction in solid fraction. Despite a monotonic loss of entropy over time after the second flow arrives, the remelting can occur as some sensible heat is converted into latent heat. In the other two regimes, the melt thickness never increases after the arrival of the second lobe.

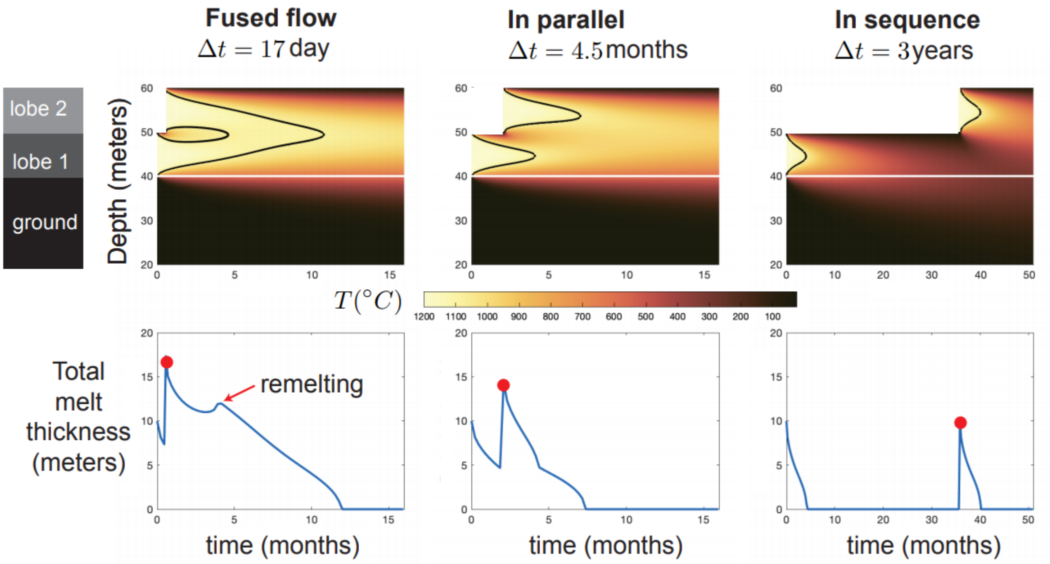

Figure 1. Emplacement of two 10m-thick lava slabs where the second slab is emplaced after 8.5 days (left), 2 months (middle) and 3 years (right). Top: Evolution of the temperature field over time. The white line marks the ground and the dark line marks the solid-liquid boundary as defined by $\phi = 0.5$. The ground portion extends between 0-40 meters (only half of the ground is shown here). Bottom: the corresponding solidified fraction of the total emplaced lava over time. The red dot marks the arrival of the second slab.

We compile the results from all the simulations into a regime diagram in Figure 2, which shows the combined control of individual flow thickness and emplacement intervals on the inter-lobe solidification during sequential emplacement. We map the three regions of inter-lobe solidification, separated by two boundaries extrapolated from our results: $t_{\text{emp}} = 0.01h^2/\alpha$ and $t_{\text{emp}} = 0.06h^2/\alpha$. These regimes and the boundaries that define them are universal for both thin and thick lobes.

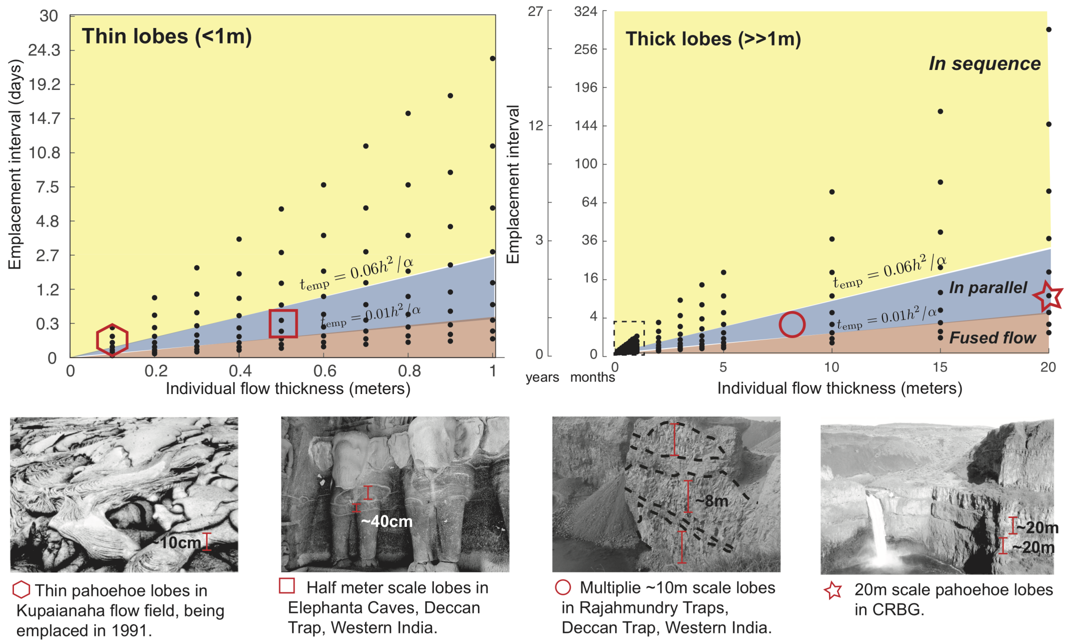

Figure 2. Regime diagram of two-lobe emplacement dynamics for different flow thickness and emplacement intervals, focusing on the dynamics for thin lobes (left) and thick lobes (right). The black dots mark the parameters we have simulated using our model. The bottom four panels illustrate examples of lava flow of various thickness that appear to have been emplaced *in parallel* or *in sequence* as suggested by their distinct inter-lobe boundaries. These examples are also marked in the regime diagrams, where the vertical position of the marker corresponds to the minimum emplacement interval predicted by our model (e.g. $t_{\text{emp}} = 0.01h^2/\alpha$). In particular, the polygonal marker corresponds to ∼10cm thin lobes as seen in Kupaianaha flow field that are predicted to be emplaced at least ∼4 minutes apart; the square marker corresponds to ∼0.5m thin lobes as seen in Elephanta Caves, and are predicted to be emplaced at least ∼2 hours apart; the circular marker corresponds to ∼8m thick lobes as seen in Rajahmundry Traps (Fendley et al., 2020a), that are predicted to be emplaced at least ∼20 days apart; the star-shaped marker corresponds to ∼20m thick lobes as seen in CRBG that are predicted to be emplaced at least ∼4 months apart.

4 Discussion

A body of literature commonly assumes that even the thickest ($>$ 40m) CFB flows were formed by flow inflation (Self et al., 1996, 1998; Anderson et al., 1999; Rader et al., 2017) based on the observations of Hawaiian lava flows (Hon et al., 1994b). However, our theoretical analysis suggests that thick (30-40 m total height) flows could also arise by fusing of flows if eruption intervals are shorter than a month or two. Fusing would remove structures that identify the crusts of the two lobes. However, some relics of the originally distinct flow may remain, such as compositional differences (Vye-Brown et al., 2013; Reidel, 2005) and possibly structures indicative of fused flow crusts such as vesicle-rich horizons and multiple entablature zones (Figure 3).

One potential example of a CFB flow that may have formed as a fused flow is the $\sim$ 70m thick Cohassett Flow from the CRFB. The flow is a member of the Grande Ronde Basalt and is a member of the Sentinel Bluffs Member lava flows in the Pascoe Basin (e.g., McMillan et al., 1989; Reidel, 2005, see Figure 3A for a map of outcrops and drill core data). As shown in the annotated picture in Figure 3B, the Cohassett has a multi-tiered structure with alternating entablatures and colonnades, as well as a 6.5m thick internal vesicular zone (IVZ, $\sim$ 20 m from the flow top, Figure 3B,C,D) with many $\sim$ 1 cm diameter vesicles (McMillan et al., 1989; Tomkeieff, 1940). The Cohassett flow exhibits one of the most striking geochemical variations amongst the Grande Ronde flows. The flow has an approximate vertical bilateral symmetry geochemically centered just under the IVZ, as seen from the data across sections more than 50 km apart (Figure 3). Using characteristic patterns in TiO_2, P_2O_5 (and other major and trace elements), Reidel (2005) defined four distinct compositional types within the flow - California Creek, Airway Heights, Stember Creek, and Spokane Falls. Typically, these compositional types are separated by a vesicular horizon. For example, a horizon $\sim$13-15 m from flow top separates massive basalt of the California Creek composition from the Airway Heights composition. Similarly, the Airway Heights and Stember Creek transition is characterized physically by a series of large vugs. The IVZ acts as the contact between the Spokane Falls and the Stember Creek compositional types (Figure 3B,C,D). Finally, a vesicular horizon $\sim$ 40 m from flow top defines the transition from the Spokane Falls back to the Stember Creek compositional types. Interestingly, the subsequent compositional type changes from Stember Creek to California Creek/Airway Heights lack clear vesicular horizons (Figure 3).

Corresponding spatially with these geochemical changes, the Cohassett flow also exhibits systematic changes in plagioclase abundance and fine-grained fraction (groundmass, Figure 3C based on data from Reidel, 2006). In particular, the flow part comprising the IVZ and the Spokane Falls composition member has a fine fraction much more indicative of a flow top rather than the flow interior. Thus, this flow interior was potentially emplaced rapidly and cooled faster than a continuously inflating flow lobe interior (McMillan et al., 1989; Philpotts & Philpotts, 2005). The IVZ-entablature-colonnade sequence in the Spokane Falls lava further supports the conclusion that the cooling rates in this part of the flow were more akin to a flow top (DeGraff et al., 1989; Forbes et al., 2014). Even on an overall flow scale, the textural data for Cohassett flow are inconsistent with the slow cooling expected for a $\sim$ 70 m flow. The plagioclase crystal size does not significantly change throughout the flow, unlike the case for a slowly cooling ponded lava lake (Philpotts & Philpotts, 2005; Cashman & Marsh, 1988).

Previously, Reidel (2005) proposed that the Cohassett flow formed by the combination of different sheet flows (for each compositional type), each sourced from a different magma reservoir and eruptive vent. These individual flows sequentially intruded into the Cohassett flow as flow lobes and inflated it to its final height. One potential challenge for this model is to explain the abrupt shift to distinct compositional types along with sharp vesicle horizons (Figure 3B, B1-B2) without any signs of magma mixing or shear instabilities despite intrusion and transport within the Cohassett flow for 10s of km. Alternatively, S. Self & Th. Thordarson (personal comm., see also Vye-Brown et al. (2013)) proposed that the Cohassett flow was formed by semi-continuous inflation with changing magma compositions in the magmatic system feeding the eruption. Philpotts and Philpotts (2005) proposed that crystal-mush compaction in an inflated sheet lobe can also partially explain the observed geochemical variation. We propose a third alternative, building upon the original idea proposed by Reidel (2005). We posit that the Cohassett flow is an example of a *fused* flow with multiple flow lobes having different compositions. Suppose the Cohassett was close to the boundary between the fused and in-parallel flow types (Figure 2). In that case, the presence of separating vesicle horizons as well as high fine-grained size fraction, especially for Spokane Falls type, can be explained. Within this scenario, each constituent $\sim$ 10-20 m lobe would have to be emplaced within a few months of the previous lobe. However, more detailed modeling work specifically focused on the Cohassett as well as textural analysis (Cashman & Marsh, 1988; Giuliani et al., 2020, e.g., stratigraphic crystal size distributions to estimate cooling rates) would be needed to ascertain which of the proposed models is correct and if Cohassett is indeed a *fused* flow.

It is similarly difficult to distinguish between *in parallel* and *in sequence* flows based on field volcanological observations alone without detailed textural analysis. One potential distinguishing feature may be the 2D shape of the bottom flow lobe in a *in parallel* flow since it will be visco-elastically deformed by the load from the overlying flow lobe (Abbott & Richards, 2020). One consequence of this would be formation of squeeze-up structures at flow lobe edges seen in some CFB flow edges (e.g., Dole et al., 2020; Fendley et al., 2020b, for the Western Ghats and the Rajahmundry Trap flows in the Deccan CFB respectively).

5 Conclusion

We provide the theoretical lower bound on emplacement interval that distinguishes a *fused flow* from non-merged flows. For instance, a distinct boundary between two lobes of 10 cm each suggests that they were emplaced at least 4 minutes apart ($t_{\mathrm{emp}} > 0.01h^2/\alpha \approx$ 4 minutes). The same calculation for two 20 m thick lobes suggests that the emplacement interval is at least 4 months if a distinct boundary is present between the two lobes. We also show the effectiveness of using phase-field models and high-order numerical schemes in simulating lava solidification problems with drastically varying timescales.

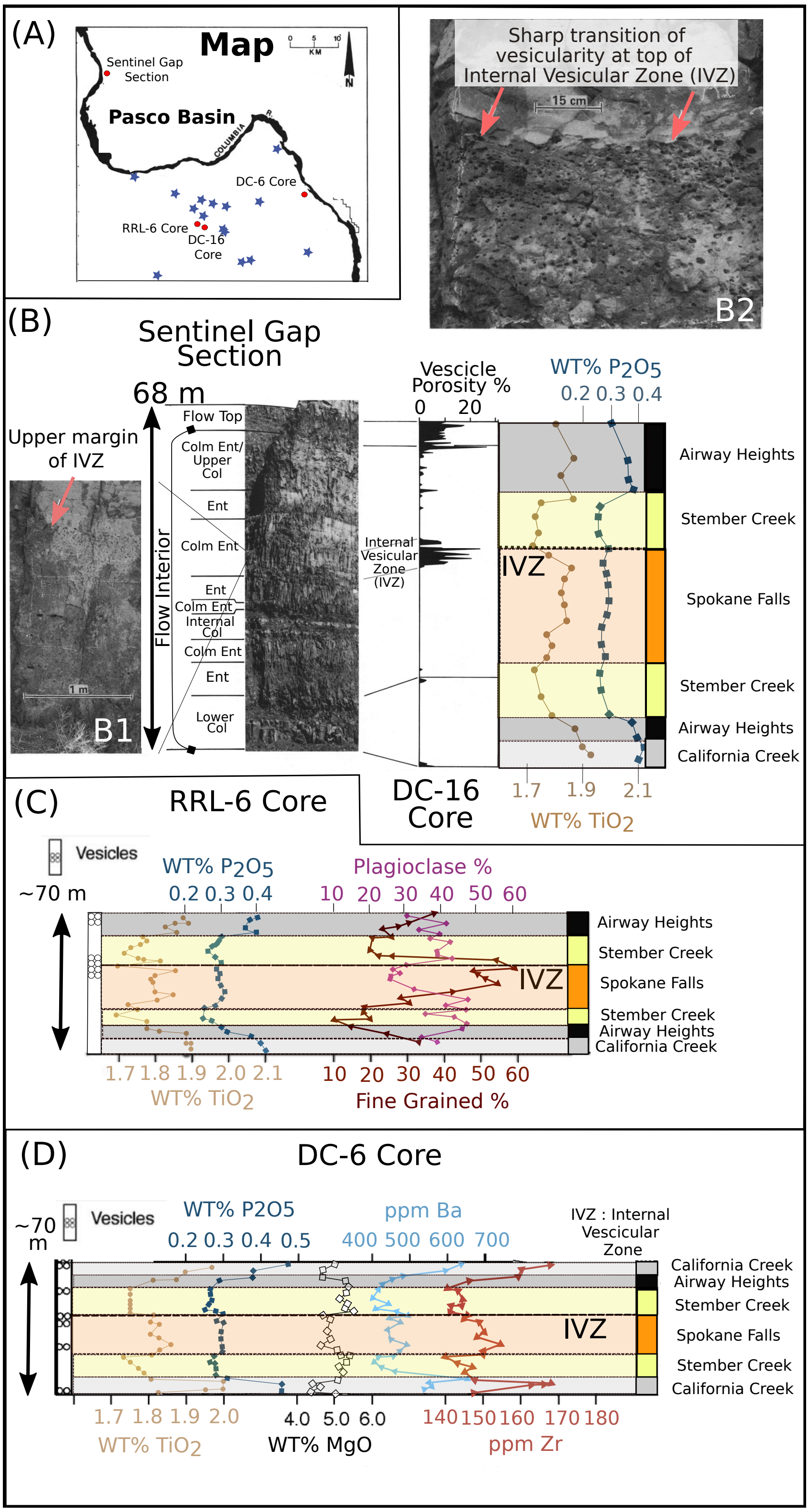

Figure 3. Stratigraphic sections for multiple Cohassett flow outcrops and cores in the Pasco Basin, Columbia River Basalts. (A) Regional Map showing the location of the sections plotted in the figure (red points) and other drill cores with similar stratigraphy (blue stars). (B) Internal stratigraphy of the Cohassett flow in the Sentinel Gap outcrop with zoom in pictures (B1, B2) showing the sharp vesicularity transitions at the Internal vesicular Zone (IVZ) ∼ 20 from the flow top (modified from McMillan et al. 1989). Colm e - Columnar, Ent - Entablature, and Col - Colonnade. The right panels show the vescicle porosity and geochemical variations in the DC-16 borehole. Panels (C) and (D) show stratigraphic section with geochemical and textural variations in the Cohassett flow in the RRl-6 Core and DC-6 cores respectively (Data from Reidel 2005). We also show the assigned compositional types to parts of the Cohassett flow by Reidel 2005

Acknowledgments

X.F. acknowledges the support of the Miller Fellowship. S.S. would like to acknowledge the support of D. Basu, K. Das and the Center for Nuclear Waste Regulatory Analyses for carrying out an earlier version of this study. M.M., S.S., and T.M. were supported by NSF 1615203. T.M. acknowledges funding support from the Crosby Postdoc Fellowship at MIT. All relevant simulation data, movies, figures, and codes can be found at `https://zenodo.org/badge/latestdoi/357729300`. In particular, all data files are contained in `finaldata.zip`, all codes can be found in the folder `finalcodes`, all relevant figures from this paper can be found in the folder `finalfigures`, and all movies (plus some extra movies) can be found in the folder `movies`.

References

Abbott, K., & Richards, M. A. (2020). Elastic flexure of young, overlapping basaltic lava flows offshore the galápagos and hawaiian islands: Observations, modeling, and thermal/chronological analysis. *Geochemistry, Geophysics, Geosystems*, *21*(3), e2019GC008864.

Anderson, D. M., McFadden, G. B., & Wheeler, A. A. (1998). Diffuse-Interface methods in fluid mechanics. *Annual Review of Fluid Mechanics*, *30*(1), 139–165.

Anderson, S. W., Stofan, E., Smrekar, S., Guest, J., & Wood, B. (1999). Pulsed inflation of pahoehoe lava flows: implications for flood basalt emplacement. *Earth and Planetary Science Letters*, *168*(1-2), 7–18.

Atkinson, K. (1988). *An Introduction to Numerical Analysis.* New York: Wiley.

Basu, D., Das, K., & Self, S. (2012). Numerical simulations and analysis of lava flow cooling [Report to US Nuclear Regulatory Commission]. (NRC 02-07-006, IM 14002.01.441.148).

Basu, D., Das, K., & Self, S. (2013). Numerical analysis of lava cooling with different geometric configurations [Report to US Nuclear Regulatory Commission]. (NRC 02-07-006 and HQ–12–C–02–0089; IM 17860.09.001.380).

Boettinger, W. J., Warren, J. a., Beckermann, C., & Karma, A. (2002). Phase-field simulation of solidification. *Annual Review of Materials Research*, *32*(1), 163–194.

Bryan, S. E., & Ernst, R. E. (2008). Revised definition of large igneous provinces (lips). *Earth-Science Reviews*, *86*(1-4), 175–202.

Cahn, J. W., & Hilliard, J. E. (1958). Free Energy of a Nonuniform System. I. Interfacial Free Energy. *The Journal of Chemical Physics*, *28*(2), 258.

Cashman, K. V., & Marsh, B. D. (1988). Crystal size distribution (csd) in rocks and the kinetics and dynamics of crystallization ii: Makaopuhi lava lake. *Contributions to Mineralogy and Petrology*, *99*(3), 292–305.

Clapham, M. E., & Renne, P. R. (2019). Flood basalts and mass extinctions. *Annual Review of Earth and Planetary Sciences*, *47*, 275–303.

DeGraff, J. M., Long, P. E., & Aydin, A. (1989). Use of joint-growth directions and rock textures to infer thermal regimes during solidification of basaltic lava flows. *Journal of Volcanology and Geothermal Research*, *38*(3-4), 309–324.

Dole, G., Patil-Pillai, S., & Kale, V. S. (2020). Multi-tiered, disrupted crust of a sheet lava flow from the diveghat formation of deccan traps: Implications on emplacement mechanisms. *Journal of Earth System Science*, *129*(1), 1–9.

Fendley, I. M., Sprain, C. J., Renne, P. R., Arenillas, I., Arz, J. A., Gilabert, V., ... Mittal, T. (2020a). No Cretaceous-Paleogene Boundary in Exposed Rajahmundry Traps: A Refined Chronology of the Longest Deccan Lava Flows From 40Ar/39Ar Dates, Magnetostratigraphy, and Biostratigraphy. *Geochemistry, Geophysics, Geosystems*, *21*(9), 1–20.

Fendley, I. M., Sprain, C. J., Renne, P. R., Arenillas, I., Arz, J. A., Gilabert, V., ... others (2020b). No cretaceous-paleogene boundary in exposed rajahmundry traps: A refined chronology of the longest deccan lava flows from 40ar/39ar dates, magnetostratigraphy, and biostratigraphy. *Geochemistry, Geophysics, Geosystems*, *21*(9), e2020GC009149.

Forbes, A. E., Blake, S., & Tuffen, H. (2014). Entablature: fracture types and mechanisms. *Bulletin of Volcanology*, *76*(5), 1–13.

Fujii, M. (1991). An extension of Milne's device for the Adams Predictor-Corrector Methods. *Japan Journal of Industrial and Applied Mathematics*, *8*(1), 1–18.

Giuliani, L., Iezzi, G., Vetere, F., Behrens, H., Mollo, S., Cauti, F., ... Scarlato, P. (2020). Evolution of textures, crystal size distributions and growth rates of plagioclase, clinopyroxene and spinel crystallized at variable cooling rates from a mid-ocean ridge basaltic melt. *Earth-Science Reviews*, *204*, 103165.

Hoblitt, R. P., Orr, T. R., Heliker, C., Denlinger, R. P., Hon, K., & Cervelli, P. F. (2012). Inflation rates, rifts, and bands in a pāhoehoe sheet flow. *Geosphere*, *8*(1), 179-195.

Hon, K., Kauahikaua, J., Denlinger, R., & Mackay, K. (1994a). Emplacement and inflation of pāhoehoe sheet flows: observations and measurements of active lava flows on Kilauea volcano, Hawaii. *Geological Society of America Bulletin*, *106*(3), 351–370.

Hon, K., Kauahikaua, J., Denlinger, R., & Mackay, K. (1994b). Emplacement and inflation of pahoehoe sheet flows: Observations and measurements of active lava flows on kilauea volcano, hawaii. *Geological Society of America Bulletin*, *106*(3), 351–370.

Kale, V. S., Dole, G., Shandilya, P., & Pande, K. (2020). Stratigraphy and correlations in deccan volcanic province, india: quo vadis? *GSA Bulletin*, *132*(3-4), 588–607.

Kauahikaua, J., Cashman, K. V., Mattox, T. N., Heliker, C. C., Hon, K. A., Mangan, M. T., & Thornber, C. R. (1998). Observations on basaltic lava streams in tubes from kilauea volcano, island of hawai'i. *Journal of Geophysical Research: Solid Earth*, *103*(B11), 27303–27323.

Kim, S. G., & Kim, W. T. (2005). Phase-Field Modeling of Solidification. In *Handbook of materials modeling* (pp. 2105–2116). Springer, Dordrecht.

McMillan, K., Long, P. E., & Cross, R. W. (1989). Vesiculation in columbia river basalts. *Geological Society of America Special Papers*, *239*, 157–168.

Patrick, M. R., Dehn, J., & Dean, K. (2004). Numerical modeling of lava flow cooling applied to the 1997 Okmok eruption: Approach and analysis. *Journal of Geophysical Research*, *109*(B3), B03202.

Philpotts, A. R., & Philpotts, D. E. (2005). Crystal-mush compaction in the cohassett flood-basalt flow, hanford, washington. *Journal of Volcanology and Geothermal Research*, *145*(3-4), 192–206.

Provatas, N., & Elder, K. (2010). *Phase-field methods in materials science and engineering* (1st ed.). Wiley.

Puffer, J. H., Block, K. A., Steiner, J. C., & Laskowich, C. (2018). Complex layering of the orange mountain basalt: New jersey, usa. *Bulletin of Volcanology*, *80*(6), 54.

Rader, E., Vanderkluysen, L., & Clarke, A. (2017). The role of unsteady effusion rates on inflation in long-lived lava flow fields. *Earth and Planetary Science Letters*, *477*, 73–83.

Ralston, A. (1962). Runge-Kutta methods with minimum error bounds. *Mathematics of Computation*, *16*(80), 431–437.

Reidel, S. P. (2005). A lava flow without a source: The cohassett flow and its compositional components, sentinel bluffs member, columbia river basalt group. *The Journal of geology*, *113*(1), 1–21.

Reidel, S. P. (2006). Comment on philpotts and philpotts (2005): Crystal-mush compaction in the cohassett flood-basalt flow, hanford, washington. *Journal of Volcanology and Geothermal Research*, *152*(1), 189–193.

Self, S., Jay, A. E., Widdowson, M., & Keszthelyi, L. P. (2008). Correlation of the deccan and rajahmundry trap lavas: Are these the longest and largest lava flows on earth? *Journal of Volcanology and Geothermal Research*, *172*(1-2), 3–19.

Self, S., Keszthelyi, L., & Thordarson, T. (1998). The importance of pāhoehoe. *Annual Review of Earth and Planetary Sciences*, *26*(1), 81–110.

Self, S., Mittal, T., & Jay, A. E. (2021). Thickness characteristics of pāhoehoe lavas in the deccan province, western ghats, india, and in continental flood basalt provinces elsewhere. *Frontiers in Earth Science*, *8*, 720.

Self, S., Schmidt, A., & Mather, T. (2014). Emplacement characteristics, time scales, and volcanic gas release rates of continental flood basalt eruptions on earth. *Geological Society of America Special Papers*, *505*.

Self, S., Thordarson, T., Keszthelyi, L., Walker, G., Hon, K., Murphy, M., ... Finnemore, S. (1996). A new model for the emplacement of columbia river basalts as large, inflated pahoehoe lava flow fields. *Geophysical Research Letters*, *23*(19), 2689–2692.

Tomkeieff, S. I. (1940). The basalt lavas of the giant's causeway district of northern ireland. *Bulletin of Volcanology*, *6*(1), 89–143.

Vye-Brown, C., Self, S., & Barry, T. (2013). Architecture and emplacement of flood basalt flow fields: case studies from the columbia river basalt group, nw usa. *Bulletin of Volcanology*, *75*(3), 697.

Wright, T. L., & Marsh, B. (2016). Quantification of the intrusion process at Kīlauea volcano, Hawai'i. *Journal of Volcanology and Geothermal Research*, *328*, 34–44.

Wright, T. L., & Okamura, R. T. (1977). *Cooling and crystallization of tholeiitic basalt, 1965 Makaopuhi Lava Lake, Hawaii* (Tech. Rep.).

Wright, T. L., Peck, D. L., & Shaw, H. R. (1972). *Kilauea Lava Lakes: Natural Laboratories for Study of Cooling, Crystallization, and Differentiation of Basaltic Magma* (Vol. 19).

Zlatev, Z. (1985). Variable stepsize variable formula methods based on predictor-corrector schemes. *Applied Numerical Mathematics*, *1*(5), 395–416.